# Comparative Analysis of Discontinuous Space Vector PWM Techniques of a Three-Phase Inverter


1. Mohammad Arif Khan , M.TECH ( Power System & Drives) Final Year student, Email- mdarif27@rediffmail.com , arif.md27@gmail.com, Ph. no. 9927669141.
2. Dr. Atif Iqbal, Reader, Department of Electrical Engineering, Aligarh Muslim University, Aligarh, 202002, Email-atif2004@gmail.com. Ph.no.9411221037.
3. Puneet Sharma, M.TECH (Power System & Drives) Final Year student, Email-erpuneet_shm@rediffmail.com. Ph. no. 9319797454.
4. M. Rizwan Khan, Lecturer , Department of Electrical Engineering, Aligarh Muslim University, Aligarh, 202002, Email- km_rizwan@rediffmail.com. Ph.no.9412545798.

**Department of Electrical Engineering,**
**Aligarh Muslim University, Aligarh, 202002**

# Comparative Analysis of Discontinuous Space Vector PWM Techniques of a Three-Phase Inverter


## Abstract

**Variable speed ac drives are nowadays the work horse of industry. To obtain variable voltage and frequency supply, inverters are the most common choice. Various pulse width modulation (PWM) techniques have been developed for three phase voltage source inverters in the last decade. Space vector PWM technique is the most popular choice due to their easier digital implementation and better dc bus utilization when compared to the most commonly used carrier-based PWM scheme. In discontinuous PWM mode one of the leg of inverter is tied to either positive or negative rail of DC bus. This paper is devoted to the development of Space vector PWM strategies in discontinuous mode for three-phase VSIs. Discontinuous Space vector PWM offer the advantage of lower switching losses which is important especially in high switching frequency applications. The paper analyses various existing discontinuous PWM techniques based on harmonic performance of the output phase voltages. The harmonic performance indices chosen are total harmonic distortion, weighted total harmonic distortion, harmonic factor and harmonic distortion factor. The performance is evaluated based on low-order harmonic content in the output phase voltages. Further few novel Space vector PWM method in discontinuous mode is proposed and analyzed. Performance comparison of the existing techniques and proposed schemes are presented. The complete space vector model of a three-phase VSI is also presented. The analysis is done using Matlab simulation.**



***Keywords*** **– Space vector, PWM, Modulation Index, Total Harmonic distortion (THD), Weighted Total Harmonic Distortion (WTHD).**

# Comparative Analysis of Discontinuous Space Vector PWM Techniques of a Three-Phase Inverter

Mohammad Arif Khan Puneet Sharma Atif Iqbal M. Rizwan Khan

Department of Electrical Engineering, Aligarh Muslim University, Aligarh, 202002

## Abstract

Variable speed ac drives are nowadays the work horse of industry. To obtain variable voltage and frequency supply, inverters are the most common choice. Various pulse width modulation (PWM) techniques have been developed for three phase voltage source inverters in the last decade. Space vector PWM technique is the most popular choice due to their easier digital implementation and better dc bus utilization when compared to the most commonly used carrier-based PWM scheme. In discontinuous PWM mode one of the leg of inverter is tied to either positive or negative rail of DC bus. This paper is devoted to the development of Space vector PWM strategies in discontinuous mode for three-phase VSIs. Discontinuous Space vector PWM offer the advantage of lower switching losses which is important especially in high switching frequency applications. The paper analyses various existing discontinuous PWM techniques based on harmonic performance of the output phase voltages. The harmonic performance indices chosen are total harmonic distortion, weighted total harmonic distortion, harmonic factor and harmonic distortion factor. The performance is evaluated based on low-order harmonic content in the output phase voltages. Further few novel Space vector PWM method in discontinuous mode is proposed and analyzed. Performance comparison of the existing techniques and proposed schemes are presented. The complete space vector model of a three-phase VSI is also presented. The analysis is done using Matlab simulation.

*Keywords* – Space vector, PWM, Modulation Index, Total Harmonic distortion (THD), Weighted Total Harmonic Distortion (WTHD).

## (1)-INTRODUCTION

Three-phase voltage source inverters are widely used in variable speed ac motor drives applications since they provide variable voltage and variable frequency output through pulse width modulation control. Continuous improvement in terms of cost and high switching frequency of power semiconductor devices and development of machine control algorithm leads to growing interest in more precise PWM techniques. Volume of work has been carried out in this direction and a review of popular techniques are presented in [1,2]. The most widely used PWM method is the carrier-based sine-triangle PWM method due to simple implementation in both analog and digital realization. However, the dc bus utilization in this method is low $(0.5V_{dc})$. This has led to the investigation into other techniques with an objective of improvement in the dc bus utilization. It is found in [3] that injection of zero sequence (third harmonic) extends the range of operation of modulator by 15.5%. The major problem associated with high power drive applications is high switching losses in inverters. To reduce switching losses a PWM technique termed as discontinuous PWM (DPWM) was developed in [4,5]. The proposed discontinuous PWM techniques were based on triangle-intersection-implementation, in which non sinusoidal modulating signal is compared with triangular carrier wave. A generalized discontinuous PWM algorithm was presented in [6] which encompasses the techniques presented in [4,5]. However, the

better visualization of the DPWM methods is obtained by using space vector theory. A generalized DPWM based on space vector theory is available in [7, 8, 9, 10]. This paper is focused on the space vector theory approach. All the discontinuous PWM strategies is based on the principle of eliminating one of the zero voltage vectors, causing the active voltage space vectors to join together in two successive half switching interval. The discontinuous PWM techniques have the advantage of eliminating one switching transition in each half switching period, consequently reducing the number of switching by one third. Alternatively, the switching frequency can be increased by 3/2 for the same inverter losses.

Another PWM technique termed as Space vector PWM based on space vector theory was proposed in [11] which offer superior performance to the carrier-based sine-triangle PWM technique in terms of higher dc bus utilization and better harmonic performance. Later on it was realized that the placement of the active and zero space vectors in each half switching period is the only difference between the carrier-based scheme and SVPWM [12].

This paper is devoted to the development of Space vector PWM strategies in discontinuous mode for three-phase VSIs. At first space vector PWM in linear region is analyzed and a review of the existing DPWM techniques based on space vector approach is presented. Based on the existing techniques three more discontinuous space vector PWM methods are proposed by rearranging the two zero vectors skillfully. A complete analysis and comparison of the existing and the proposed techniques are presented. The performance indices chosen are the harmonic distortion factor, total harmonic distortion, weighted total harmonic distortion and harmonic switching losses.

## (2)-SPACE VECTOR PWM IN LINEAR RANGE

This section is devoted to the development of Space vector PWM for a two-level voltage source inverter in linear region of operation [7]. As seen from Fig 1, there are six switching devices and only three of them are independent as the operation of two power switches of the same leg are complimentary. The combination of these three switching states gives out eight possible space voltage vectors. The space vectors forms a hexagon with 6 distinct sectors, each spanning 60 degrees in space. At any instant of time, the inverter can produce only one space vector. In space vector PWM a set of three vectors (two active and a zero) can be selected to synthesize the desired voltage in each switching period. All of the eight modes are shown in Table.1.

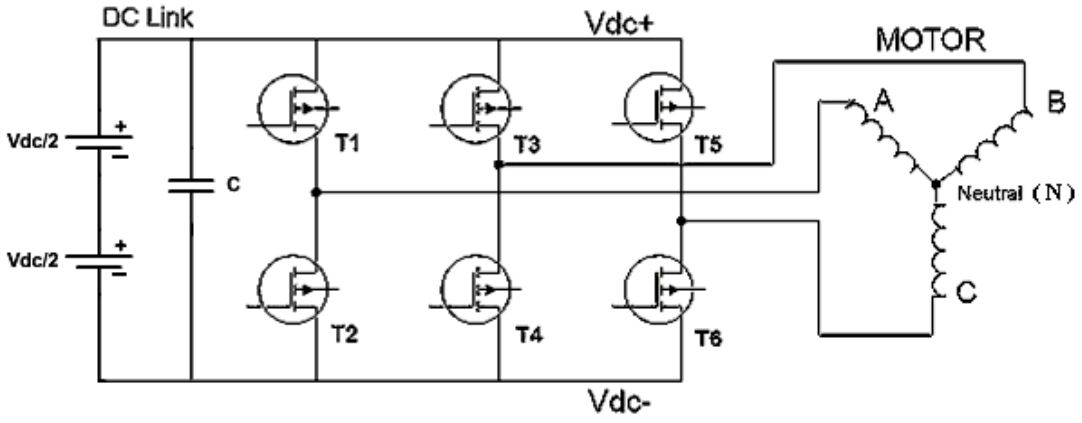


Fig. 1 Power circuit of a three-phase voltage source inverter

Table-1 Possible modes of operation of a three-phase VSI

| State | On Devices | Van | Vbn | Vcn | Space Voltage Vector |
|---|---|---|---|---|---|
| 0 | T2, T4, T6 | 0 | 0 | 0 | $V_0(000)$ |
| 1 | T1, T4, T6 | 2Vdc/3 | -Vdc/3 | -Vdc/3 | $V_1(100)$ |
| 2 | T1, T3, T6 | Vdc/3 | Vdc/3 | -2Vdc/3 | $V_2(110)$ |
| 3 | T3, T2, T6 | -Vdc/3 | 2Vdc/3 | -Vdc/3 | $V_3(010)$ |
| 4 | T2, T3, T5 | -2Vdc/3 | Vdc/3 | Vdc/3 | $V_4(011)$ |
| 5 | T2, T4, T5 | -Vdc/3 | -Vdc/3 | 2Vdc/3 | $V_5(001)$ |
| 6 | T1, T4, T5 | Vdc/3 | -2Vdc/3 | Vdc/3 | $V_6(101)$ |
| 7 | T1, T3, T5 | 0 | 0 | 0 | $V_7(111)$ |

Out of eight topologies six (states 1-6) produce a non-zero output voltage and are known as active voltage vectors and the remaining two topologies (states 0 and 7) produce zero output voltage (when the motor is shorted through the upper or lower transistors) and are known as zero voltage vectors, various possible switching states are shown in Fig 2.

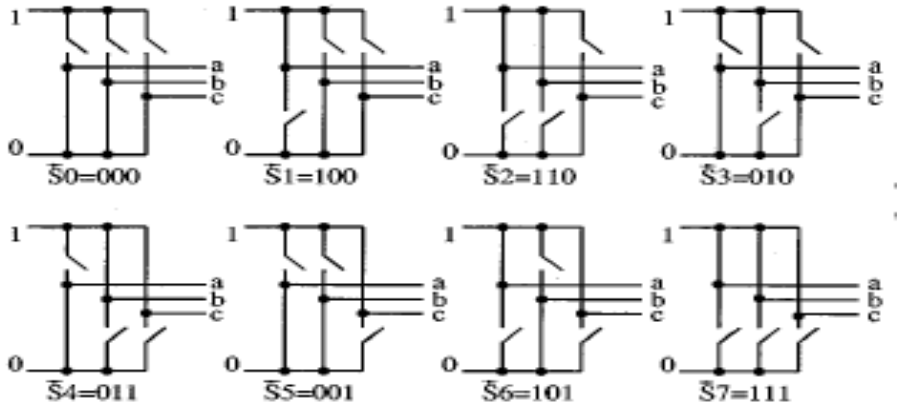


Fig. 2 -The switches position during eight topologies

Space vector is defined as [7],

$$\underline{v}_s^* = \frac{2}{3}\left(v_a + \underline{a}v_b + \underline{a}^2 v_c\right) \tag{1}$$

Where $\underline{a} = \exp\left(j2\pi/3\right)$.

The space vector is a simultaneous representation of all the three-phase quantities. It is a complex variable and is function of time in contrast to the phasors. Phase-to-neutral voltages of a star-connected load are most easily found by defining a voltage difference between the star point *n* of the load and the negative rail of the dc bus *N*. The following correlation then holds true:

$$\begin{aligned} v_A &= v_a + v_{nN} \\ v_B &= v_b + v_{nN} \\ v_C &= v_c + v_{nN} \end{aligned} \tag{2}$$

Since the phase voltages in a start connected load sum to zero, summation of equation (2) yields

$$v_{nN} = \left(1/3\right)\left(v_A + v_B + v_C\right) \tag{3}$$

Substitution of (3) into (2) yields phase-to-neutral voltages of the load in the following form:

$$\begin{aligned} v_a &= (2/3)v_A - (1/3)(v_B + v_C) \\ v_b &= (2/3)v_B - (1/3)(v_A + v_C) \\ v_c &= (2/3)v_C - (1/3)(v_B + v_A) \end{aligned} \tag{4}$$

Phase voltages are summarized and their corresponding space vectors are listed in Table 1. The eight vectors including the zero voltage vectors can be expressed geometrically as shown in Fig 3.

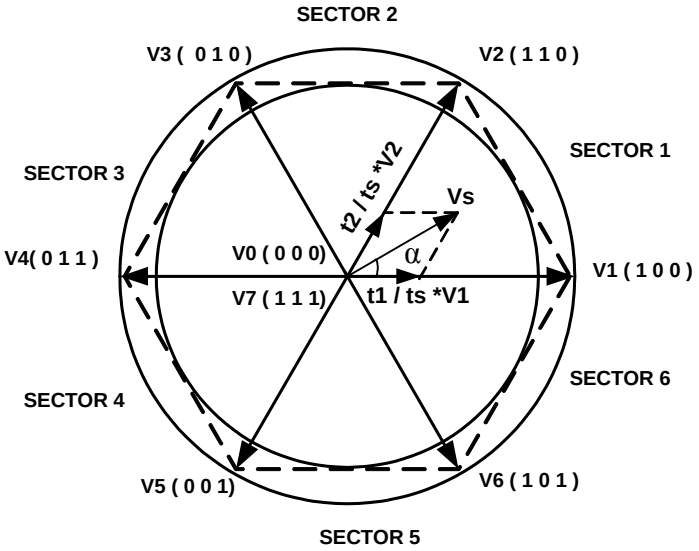


Fig. 3 - Space Vector representation of Line to Neutral Voltages

Each of the space vectors, in the diagram represent the six voltage steps developed by the inverter with the zero voltages $V_0$(0 0 0) and $V_7$(1 1 1 ) located at the origin.

Space Vector PWM require to averaging of the adjacent vectors in each sector. Two adjacent vectors and zero vectors are used to synthesis the input reference determined from Fig.4 for sector I. Using the appropriate PWM signals a vector is produced that transitions smoothly between sectors and thus provide sinusoidal line to line voltages to the motor. The switching patterns for switches in different sectors are as shown in Fig. 5.

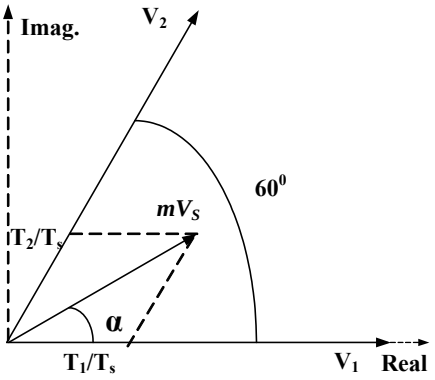


Fig. 4- Principle of time calculation for SVPWM in sector I

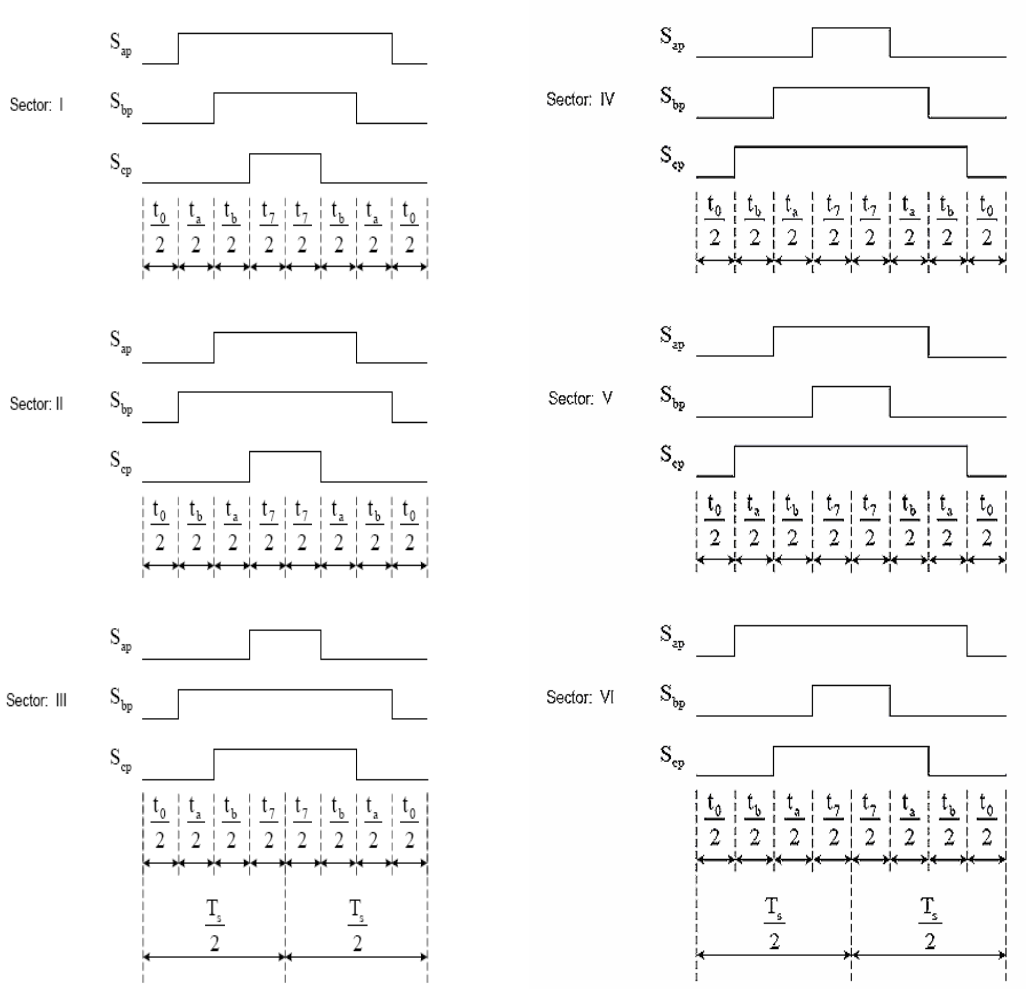


Fig. 5 - Switching Patterns for Switches in Different Sectors

In order to generate the PWM signals that produces the rotating vector. The PWM time intervals for each sector is determined from Fig. 4 for sector I as

Along real axis:

$$V_1 \frac{T_1}{T_s} + (V_2 \cos 60)\frac{T_2}{T_s} = mV_S \cos\alpha \tag{5}$$

Along imaginary axis:

$$0 + (V_2 \sin 60)\frac{T_2}{T_s} = mV_S \sin\alpha \tag{6}$$

Solving equations (5) and (6)

$$T_1 = T_S \frac{mV_S \sin(60-\alpha)}{V_1 \sin 60}$$

$$T_1 = T_s \frac{m \frac{1}{2} V_{DC} \sin(60 - \alpha)}{\frac{2}{3} V_{DC} \sin 60}$$

$$\boxed{T_1 = \frac{\sqrt{3}}{2} m T_S \sin(60 - \alpha)} \quad (7)$$

$$T_2 = T_S \frac{m V_S \sin \alpha}{V_2 \sin 60}$$

$$\boxed{T_2 = \frac{\sqrt{3}}{2} m T_S \sin(\alpha)} \quad (8)$$

$$\boxed{T_0 + T_7 = T_s - (T_1 + T_2)} \quad (9)$$

Generalizing the time expressions gives

$$T_1 = \frac{\sqrt{3}}{2} mTs \sin\left(\frac{k\pi}{3} - \alpha\right) \quad (10)$$

$$T_2 = \frac{\sqrt{3}}{2} mTs \sin\left(\frac{(k-1)\pi}{3} - \alpha\right); \text{ k=1, 2, 3…} \quad (11)$$

The time of application of active and zero space vectors for all six sectors are given in Table 2 [13]. The periods $T_1$, $T_2$ and $T_0$ depends only on the reference vector amplitude Vs and the angle '$\alpha$'. This shows that the period $T_1$, $T_2$ and $T_0$ are the same in all sectors for the same $V_S$ and '$\alpha$' position. In the under modulation region, the vector $V_S$ always remains within the hexagon. The mode ends in the upper limit when $V_S$ describes the inscribed circle of the hexagon.

Modulation Index *MI* ***(m)*** is given by

$$m = \frac{Vs^*}{V_{1Sixstep}}$$

Where, $V_S$ = input reference vector magnitude

$V_{1Six\ step}$ = fundamental peak value $\frac{2V_{DC}}{\pi}$ of the six step output.

The maximum value of input reference is the radius of largest circle inscribed in the hexagon given by

$$V_s^* = \frac{2}{3} V_{DC} \cos(30^0) = 0.577 V_{DC}$$

Therefore, maximum modulation index

$$\boxed{m = \frac{Vs^*}{V_{1SW}} = \frac{0.577 V_{DC}}{\frac{2}{\pi} V_{DC}} = 0.907} \quad (12)$$

This means that 90.7% of the fundamental of the six step wave is available in the linear region, compared to 78.55% in the sinusoidal PWM [7].

Table 2 – Application of time [13]

| Sector I<br>$(0 \le \omega t \le \frac{\pi}{3})$ | Sector II<br>$(\frac{\pi}{3} \le \omega t \le \frac{2\pi}{3})$ | Sector III<br>$(\frac{2\pi}{3} \le \omega t \le \pi)$ |
|---|---|---|
| $T_1 = \frac{\sqrt{3}}{2} m T_s \cos(\omega t + \frac{\pi}{6})$<br>$T_2 = \frac{\sqrt{3}}{2} m T_s \cos(\omega t + \frac{3\pi}{2})$<br>$T_0 + T_7 = T_s - T_1 - T_2$ | $T_2 = \frac{\sqrt{3}}{2} m T_s \cos(\omega t + \frac{11\pi}{6})$<br>$T_3 = \frac{\sqrt{3}}{2} m T_s \cos(\omega t + \frac{7\pi}{6})$<br>$T_0 + T_7 = T_s - T_2 - T_3$ | $T_3 = \frac{\sqrt{3}}{2} m T_s \cos(\omega t + \frac{3\pi}{2})$<br>$T_4 = \frac{\sqrt{3}}{2} m T_s \cos(\omega t + \frac{5\pi}{6})$<br>$T_0 + T_7 = T_s - T_3 - T_4$ |
| **Sector IV**<br>$(\pi \le \omega t \le \frac{4\pi}{3})$ | **Sector V**<br>$(\frac{4\pi}{3} \le \omega t \le \frac{5\pi}{3})$ | **Sector VI**<br>$(\frac{5\pi}{3} \le \omega t \le 2\pi)$ |
| $T_4 = \frac{\sqrt{3}}{2} m T_s \cos(\omega t + \frac{7\pi}{6})$<br>$T_5 = \frac{\sqrt{3}}{2} m T_s \cos(\omega t + \frac{\pi}{2})$<br>$T_0 + T_7 = T_s - T_4 - T_5$ | $T_5 = \frac{\sqrt{3}}{2} m T_s \cos(\omega t + \frac{5\pi}{6})$<br>$T_6 = \frac{\sqrt{3}}{2} m T_s \cos(\omega t + \frac{\pi}{6})$<br>$T_0 + T_7 = T_s - T_5 - T_6$ | $T_6 = \frac{\sqrt{3}}{2} m T_s \cos(\omega t + \frac{\pi}{2})$<br>$T_1 = \frac{\sqrt{3}}{2} m T_s \cos(\omega t + \frac{11\pi}{6})$<br>$T_0 + T_7 = T_s - T_1 - T_6$ |

# 3 - DISCONTINUOUS SPACE VECTOR PWM TECHNIQUES

It is possible to move the position of the active voltage pulses around within the half switches interval, to eliminate one zero output voltage pulse. Modulation strategies using this concept are termed discontinuous modulation, and a number of possible alternatives for three phase inverter system have been reported over the years.[7,8,9]. However, all the schemes essentially just rearrange the placement of the zero output voltage pulse within each half carrier or carrier interval.

### 3.1 Existing discontinuous modulation strategies:

It can be seen from the literature review [14], that there exist six different types of discontinuous PWM methods.

1. $t_0 = 0$ (DPWMMAX) for all sectors[15]
2. $t_7 = 0$ (DPWMMIN) for all sectors[15]
3. $0^0$ Discontinuous modulation (DPWM 0)[8]
4. $30^0$ Discontinuous modulation ( DPWM 1) [4]
5. $60^0$ Discontinuous modulation ( DPWM 2 )[8]
6. $90^0$ Discontinuous modulation ( DPWM 3)[8]

All the existing schemes are shown in figures, Fig 6. Part (a) of Fig 6 show the placement of zero vectors and part (b) of Fig 6 show the waveforms for each schemes where $V_{avg}$ (pole voltage), $V_a$ (phase voltage), $V_{nN}$(voltage between neutral point) called common mode voltage.

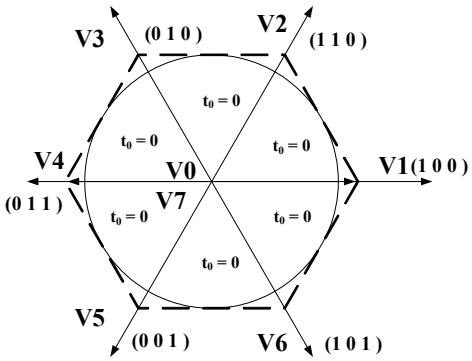


(a)

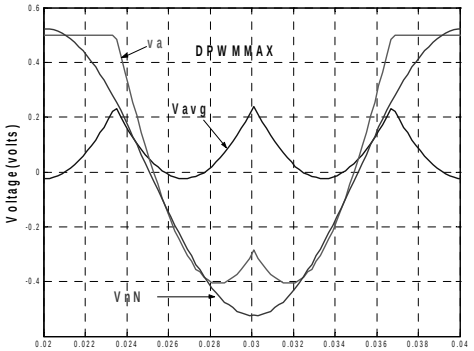


(b)

**DPWMMAX**

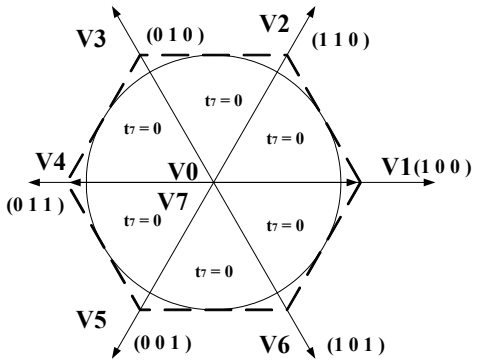


(a)

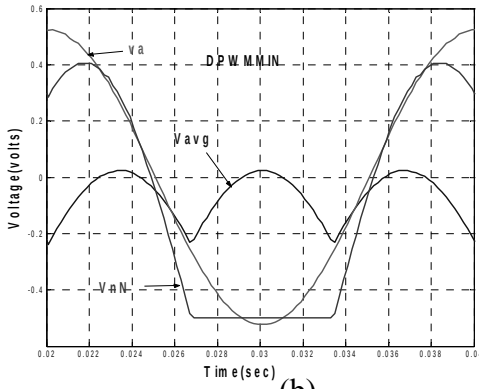


(b)

**DPWMMIN**

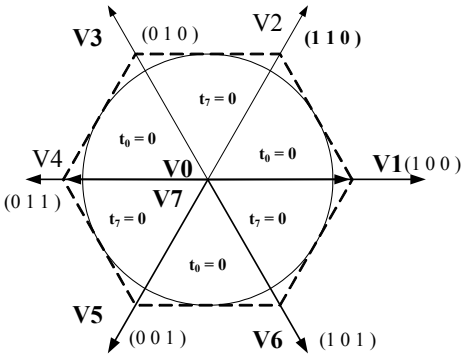


(a)

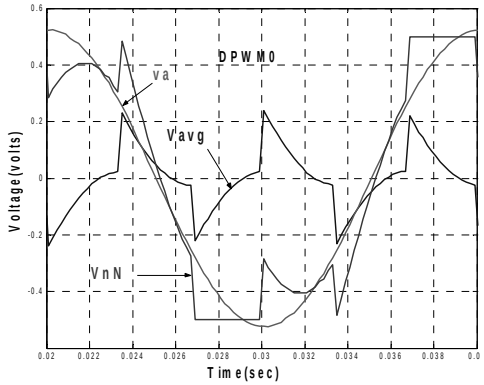


(b)

**DPWM0**

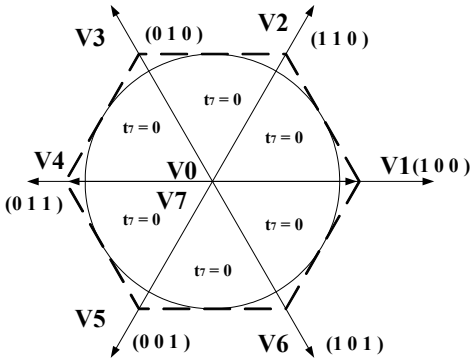


(a)

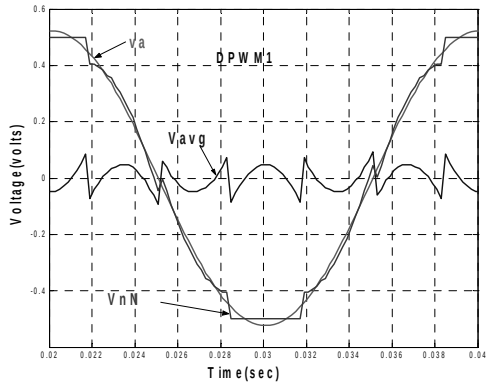


(b)

**DPWM1**

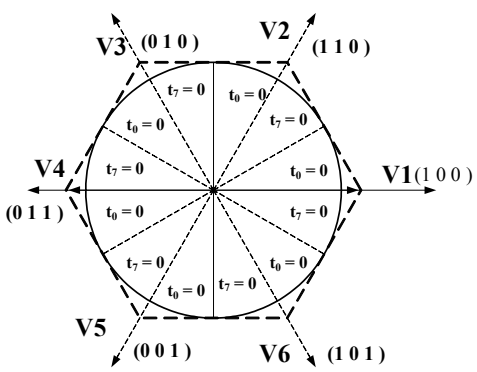


(a)

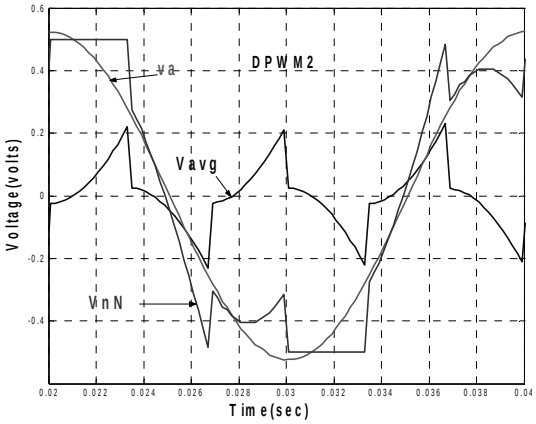


(b)

**DPWM2**

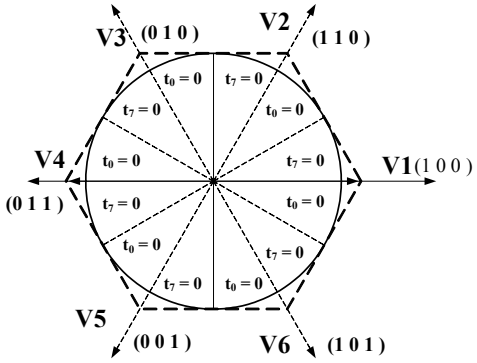


(a)

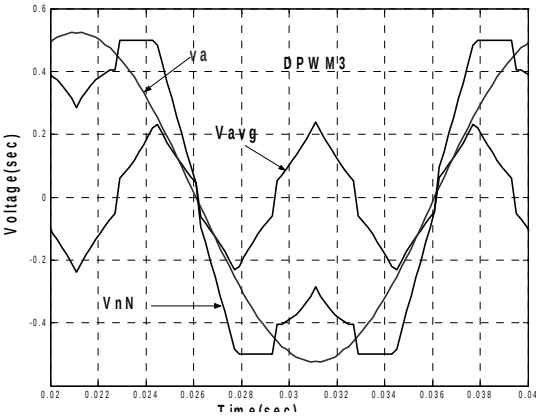


(b)

**DPWM3**

Fig. 6 Existing Discontinuous PWM schemes and associated voltage waveforms

### 3.2 Proposed Discontinuous PWM Strategies:

Based on the previously discussed methods of DPWM, three novel schemes are suggested. These are simply extension of the existing methods. The first scheme termed as DPWM4 divides the complete space vector plane in four quadrants. The zero time $t_0$ (0 0 0) is kept zero in the first and third quadrant. The zero time $t_7$ (1 1 1) is kept zero in the second and fourth quadrant. The resulting waveform of phase leg voltages and common mode voltage is shown in Fig. 7 (b). Fig 7(a) illustrates the placement of zero vectors.

The second proposed scheme keeps $t_0$ (0 0 0) is zero in first three sectors and $t_7$ (1 1 1) is remained zero for the next three sectors. The resulting waveforms are shown in Fig. 7 (c) and 7(d). This scheme is termed as .DPWM5.

In the third proposed scheme, termed as DPWM6, the complete space vector is divided into eight sectors each spanning $45^0$ .The zero vector $t_0$ (0 0 0) is kept zero in the first sector [ $0^0$ - $45^0$ ] and $t_7$ (1 1 1) is kept zero in the next sector [ $45^0$.- $90^0$.] and the pattern repeats in the subsequent sectors. The resulting waveforms are fig. 7(e) & 7 (f).

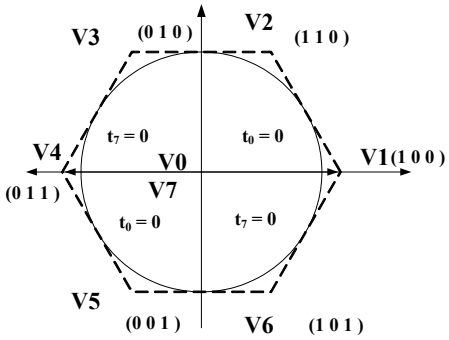


(a)

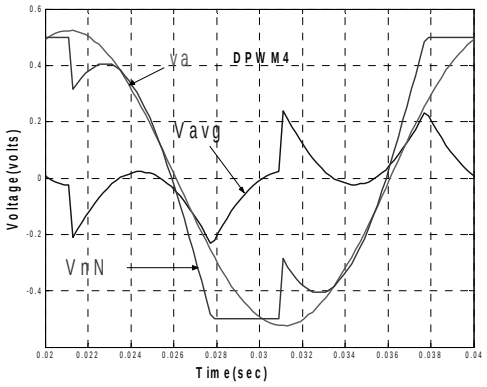


(b)

**DPWM4**

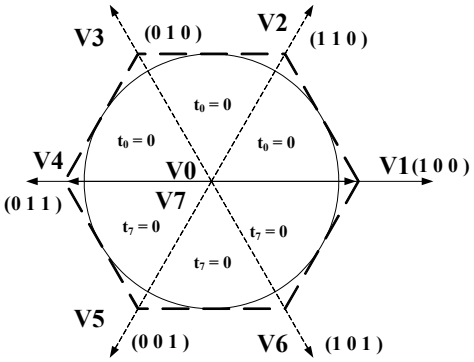


(c)

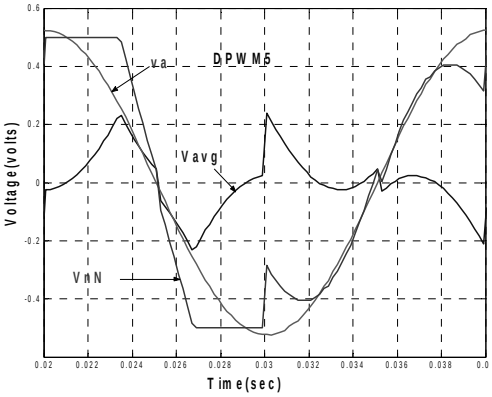


(d)

**DPWM5**

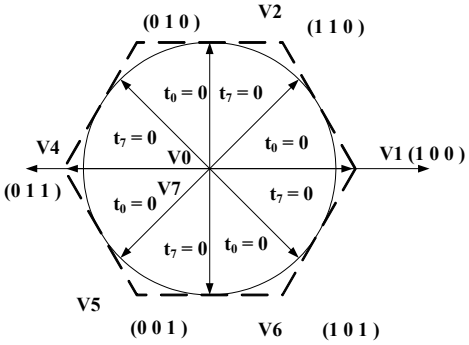


(e)

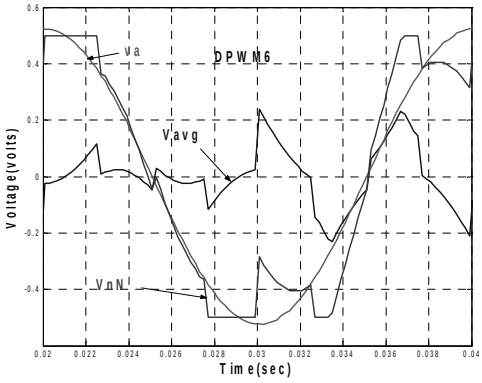


(f)

**DPWM6**

Fig. 7 Proposed discontinuous schemes and associated wave forms

## 4-Performance evaluation of DPWM schemes:

This section investigates the performance of different PWM strategies. At first average leg voltage for each sector is determined followed by the harmonic performance evaluation. Only first existing scheme namely DPWMMIN is considered for showing the sample calculation. To determine the average leg voltage considering Fig. 8 which shows the leg voltage waveform in sector I for one switching period. The positive and negative dc rail is assumed as ± *Vdc*.

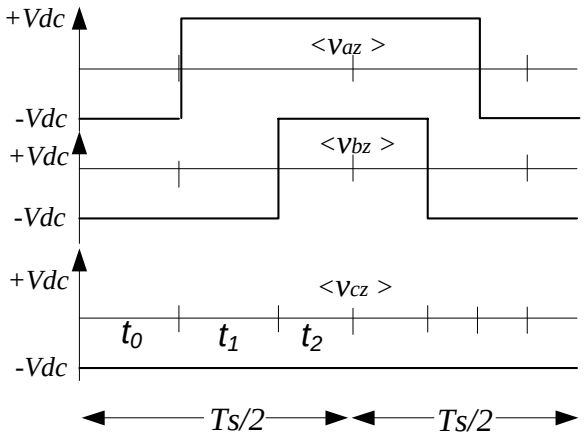


Fig 8 Pulse pattern for the DPWMMIN in the first sextant, 0<θ< π / 3

The three-phase average leg voltages can now be expressed as

$$\langle v_{az} \rangle = V_{dc}\,\frac{2}{Ts}\left(T_1 + T_2 - T_0\right) \tag{13}$$

$$\langle v_{bz} \rangle = V_{dc}\,\frac{2}{Ts}\left(-T_1 + T_2 - T_0\right) \tag{14}$$

$$\langle v_{cz} \rangle = V_{dc}\,\frac{2}{Ts}\left(-T_1 - T_2 - T_0\right) \tag{15}$$

However, since

$$\left(T_1 + T_2 - T_0\right) = \frac{Ts}{2} \tag{16}$$

The equations becomes

$$\langle v_{az} \rangle = 2V_{dc}\left(\frac{2}{Ts}T_1 + \frac{2}{Ts}T_2 - \frac{1}{2}\right) \tag{17}$$

$$\langle v_{bz} \rangle = 2V_{dc}\left(\frac{2}{Ts}T_2 - \frac{1}{2}\right) \tag{18}$$

$$\langle v_{cz} \rangle = -V_{dc} \tag{19}$$

from Table 2 substituting the values of $T_1$ & $T_2$, the three phase leg voltages becomes,

$$\langle v_{az} \rangle = V_{dc}\left[\sqrt{3}M\cos\left(\theta - \frac{\pi}{6}\right) - 1\right];\ 0 \le \theta \le 2\,\pi/3 \tag{20}$$

$$\langle v_{bz} \rangle = V_{dc}\left[\sqrt{3}M\cos\left(\theta - \frac{\pi}{2}\right) - 1\right];\ 0 \le \theta \le 2\pi/3 \tag{21}$$

$$\langle v_{cz} \rangle = -V_{dc};\ 0 \le \theta \le \pi/3 \tag{22}$$

The result expression for average leg voltage for all six sectors are tabulated in Table 3

Table 3: Average Leg voltages for $t_7 = 0$ **DPWMMIN**

| $60^0$ Sextant | Phase Leg a $\langle v_{az} \rangle / V_{dc}$ | Phase Leg b $\langle v_{bz} \rangle / V_{dc}$ | Phase Leg c $\langle v_{cz} \rangle / V_{dc}$ |
|---|---|---|---|
| $2\pi/3 < \theta < \pi$ | -1 | $-1 - \sqrt{3}\, M \cos\left(\theta - \frac{\pi}{6}\right)$ | $-1 + \sqrt{3}\, M \cos\left(\theta + \frac{5\pi}{6}\right)$ |
| $0 \le \theta \le 2\pi/3$ | $-1 - \sqrt{3}\, M \cos\left(\theta + \frac{5\pi}{6}\right)$ | $-1 + \sqrt{3}\, M \sin\theta$ | -1 |
| $-2\pi/3 \le \theta \le 0$ | $-1 + \sqrt{3}\, M \cos\left(\theta + \frac{\pi}{6}\right)$ | -1 | $-1 - \sqrt{3}\, M \sin\theta$ |
| $-\pi \le \theta \le -2\pi/3$ | -1 | $-1 - \sqrt{3}\, M \cos\left(\theta + \frac{\pi}{6}\right)$ | $-1 + \sqrt{3}\, M \cos\left(\theta + \frac{5\pi}{6}\right)$ |

Following the same principle, average leg voltage for other scheme is evaluated and the resulting expression are tabulating in table 4 – 10.

Table 4: Average Leg voltages for **DPWMMAX**

| $60^0$ Sextant | Phase Leg a $\langle v_{az} \rangle / V_{dc}$ | Phase Leg b $\langle v_{bz} \rangle / V_{dc}$ | Phase Leg c $\langle v_{cz} \rangle / V_{dc}$ |
|---|---|---|---|
| $2\pi/3 < \theta < \pi$ | $\frac{3}{2} M \cos\theta - \sqrt{3} M \sin\theta + 1$ | 1 | $-\sqrt{3} M \sin\theta + 1$ |
| $\pi/3 \le \theta \le 2\pi/3$ | $\frac{\sqrt{3}}{2} M \cos(\theta + \frac{\pi}{6}) + 1$ | 1 | $-\sqrt{3} M \sin\theta + 1$ |
| $0 \le \theta \le \pi/3$ | 1 | $-\frac{\sqrt{3}}{2} M \cos(\theta + \frac{\pi}{6}) + 1$ | $-\frac{3}{2} M \cos\theta - \sqrt{3} M \sin\theta + 1$ |
| $-\pi/3 \le \theta \le 0$ | 1 | $\sqrt{3} M \sin\theta + 1 - \frac{3}{2} M \cos\theta$ | $\frac{\sqrt{3}}{2} M \sin\theta + 1$ |
| $-2\pi/3 \le \theta \le -\pi/3$ | $\frac{\sqrt{3}}{2} M \sin\frac{\theta}{3} + 1$ | $\frac{\sqrt{3}}{2} M \sin\theta + 1$ | 1 |
| $-\pi \le \theta \le -2\pi/3$ | $\frac{3}{2} M \cos\theta + \frac{\sqrt{3}}{2} M \sin\theta + 1$ | $\frac{\sqrt{3}}{2} M \sin\theta + 1$ | 1 |

Table 5: Average Leg voltages for **DPWM0**

| $60^0$ Sextant | Phase Leg a $\langle v_{az} \rangle / V_{dc}$ | Phase Leg b $\langle v_{bz} \rangle / V_{dc}$ | Phase Leg c $\langle v_{cz} \rangle / V_{dc}$ |
|---|---|---|---|
| $2\pi/3 < \theta < \pi$ | -1 | $\frac{\sqrt{3}}{2} M \sin\theta - \frac{3}{2} M \cos\theta - 1$ | $-\frac{\sqrt{3}}{2} M \sin\frac{\theta}{3} - 1$ |
| $\pi/3 \leq \theta \leq 2\pi/3$ | $\frac{\sqrt{3}}{2} M \cos(\theta + \frac{\pi}{6}) + 1$ | 1 | $-\frac{\sqrt{3}}{2} M \sin\theta + 1$ |
| $0 \leq \theta \leq \pi/3$ | $\frac{\sqrt{3}}{2} M \cos(\theta + \frac{\pi}{6}) - 1$ | $\frac{\sqrt{3}}{2} M \sin\theta - 1$ | -1 |
| $-\pi/3 \leq \theta \leq 0$ | 1 | $\frac{\sqrt{3}}{2} M \sin\theta - \frac{3}{2} M \cos\theta + 1$ | $\frac{\sqrt{3}}{2} M \sin\theta - \frac{3}{2} M \cos\theta - 1$ |
| $-2\pi/3 \leq \theta \leq -\pi/3$ | $\frac{\sqrt{3}}{2} M \cos(\theta + \frac{\pi}{6}) - 1$ | -1 | $-\frac{\sqrt{3}}{2} M \sin\theta - 1$ |
| $-\pi \leq \theta \leq -2\pi/3$ | $\frac{3}{2} M \cos\theta + \frac{\sqrt{3}}{2} M \sin\theta + 1$ | $\frac{\sqrt{3}}{2} M \sin\theta + 1$ | 1 |

Table 6: Average Leg voltages for **DPWM1**

| $60^0$ Sextant | Phase Leg a $\langle v_{az} \rangle / V_{dc}$ | Phase Leg b $\langle v_{bz} \rangle / V_{dc}$ | Phase Leg c $\langle v_{cz} \rangle / V_{dc}$ |
|---|---|---|---|
| $5\pi/6 < \theta < \pi$ | -1 | $-1 - \sqrt{3} M \cos\left(\theta + \frac{\pi}{6}\right)$ | $-1 + \sqrt{3} M \cos\left(\theta + \frac{5\pi}{6}\right)$ |
| $\pi/2 \leq \theta \leq 5\pi/6$ | $+1 + \sqrt{3} M \cos\left(\theta + \frac{\pi}{6}\right)$ | +1 | $+1 - \sqrt{3} M \sin\theta$ |
| $\pi/6 \leq \theta \leq \pi/2$ | $-1 - \sqrt{3} M \cos\left(\theta + \frac{5\pi}{6}\right)$ | $-1 + \sqrt{3} M \sin\theta$ | -1 |
| $-\pi/6 \leq \theta \leq \pi/6$ | + 1 | $+1 - \sqrt{3} M \cos\left(\theta + \frac{\pi}{6}\right)$ | $+1 + \sqrt{3} M \cos\left(\theta + \frac{5\pi}{6}\right)$ |
| $-\pi/2 \leq \theta \leq -\pi/6$ | $-1 + \sqrt{3} M \cos\left(\theta + \frac{\pi}{6}\right)$ | -1 | $-1 - \sqrt{3} M \sin\theta$ |
| $-5\pi/6 \leq \theta \leq -\pi/2$ | $+1 - \sqrt{3} M \cos\left(\theta + \frac{5\pi}{6}\right)$ | $+1 + \sqrt{3} M \sin\theta$ | +1 |
| $-\pi \leq \theta \leq -5\pi/6$ | -1 | $-1 - \sqrt{3} M \cos\left(\theta + \frac{\pi}{6}\right)$ | $-1 + \sqrt{3} M \cos\left(\theta + \frac{5\pi}{6}\right)$ |

Table 7: Average Leg voltages for **DPWM2**

| $60^0$ Sextant | Phase Leg a $\langle v_{az} \rangle / V_{dc}$ | Phase Leg b $\langle v_{bz} \rangle / V_{dc}$ | Phase Leg c $\langle v_{cz} \rangle / V_{dc}$ |
|---|---|---|---|
| $2\pi/3 < \theta < \pi$ | $\frac{3}{2}M\cos\theta - \frac{\sqrt{3}}{2}M\sin\theta + 1$ | 1 | $-\frac{\sqrt{3}}{2}M\sin\theta + 1$ |
| $\pi/3 \le \theta \le 2\pi/3$ | $\frac{\sqrt{3}}{2}M\sin(\theta - \frac{\pi}{3}) - 1$ | $\frac{\sqrt{3}}{2}M\sin\theta - 1$ | -1 |
| $0 \le \theta \le \pi/3$ | 1 | $\frac{\sqrt{3}}{2}M\cos(\theta + \frac{\pi}{6})$ - 1 | $-\frac{3}{2}M\cos\theta - \frac{\sqrt{3}}{2}M\sin\theta + 1$ |
| $-\pi/3 \le \theta \le 0$ | $-\frac{\sqrt{3}}{2}M\sin\theta + \frac{3}{2}M\cos\theta$ -1 | -1 | $\frac{\sqrt{3}}{2}M\sin(\theta + \frac{\pi}{3}) - 1$ |
| $-2\pi/3 \le \theta \le -\pi/3$ | $\frac{\sqrt{3}}{2}M\sin(\theta + \frac{\pi}{3}) + 1$ | $\frac{\sqrt{3}}{2}M\sin\theta + 1$ | 1 |
| $-\pi \le \theta \le -2\pi/3$ | -1 | $-\frac{\sqrt{3}}{2}M\cos(\theta + \frac{\pi}{6})$ -1 | $-\frac{3}{2}M\cos\theta - \frac{\sqrt{3}}{2}M\sin\theta + 1$ |

Table 8: Average Leg voltages for **DPWM3**

| $60^0$ Sextant | Phase Leg a $\langle v_{az} \rangle / V_{dc}$ | Phase Leg b $\langle v_{bz} \rangle / V_{dc}$ | Phase Leg c $\langle v_{cz} \rangle / V_{dc}$ |
|---|---|---|---|
| $2\pi/3 < \theta < \pi$ | -1 | $-1 - \sqrt{3}M\cos\left(\theta + \frac{\pi}{6}\right)$ | $-1 + \sqrt{3}M\cos\left(\theta + \frac{5\pi}{6}\right)$ |
| $\pi/3 \le \theta \le 2\pi/3$ | $+1 + \sqrt{3}M\cos\left(\theta + \frac{\pi}{6}\right)$ | +1 | $+1 - \sqrt{3}M\sin\theta$ |
| $0 \le \theta \le \pi/3$ | $-1 - \sqrt{3}M\cos\left(\theta + \frac{5\pi}{6}\right)$ | $-1 + \sqrt{3}M\sin\theta$ | -1 |
| $-\pi/3 \le \theta \le 0$ | +1 | $+1 - \sqrt{3}M\cos\left(\theta + \frac{\pi}{6}\right)$ | $+1 + \sqrt{3}M\cos\left(\theta + \frac{5\pi}{6}\right)$ |
| $-2\pi/3 \le \theta \le -\pi/3$ | $-1 + \sqrt{3}M\cos\left(\theta + \frac{\pi}{6}\right)$ | -1 | $-1 - \sqrt{3}M\sin\theta$ |
| $-\pi \le \theta \le -2\pi/3$ | $+1 - \sqrt{3}M\cos\left(\theta + \frac{5\pi}{6}\right)$ | $+1 + \sqrt{3}M\sin\theta$ | +1 |

Table 9: Average Leg voltages for **DPWM4**

| $60^0$ Sextant | Phase Leg a $\langle v_{az} \rangle / V_{dc}$ | Phase Leg b $\langle v_{bz} \rangle / V_{dc}$ | Phase Leg c $\langle v_{cz} \rangle / V_{dc}$ |
|---|---|---|---|
| $2\pi/3 < \theta < \pi$ | $\frac{3}{2} M \cos\theta - \frac{\sqrt{3}}{2} M \sin\theta + 1$ | 1 | $-\frac{\sqrt{3}}{2} M \sin\theta + 1$ |
| $\pi/3 \leq \theta \leq 2\pi/3$ | $\frac{\sqrt{3}}{2} M \cos(\theta + \frac{\pi}{6}) + 1$ | 1 | $-\frac{\sqrt{3}}{2} M \sin\theta + 1$ |
| $0 \leq \theta \leq \pi/3$ | 1 | $-\frac{\sqrt{3}}{2} M \cos(\theta + \frac{\pi}{6}) - 1$ | $-\frac{3}{2} M \cos\theta - \frac{\sqrt{3}}{2} M \sin\theta + 1$ |
| $-\pi/3 \leq \theta \leq 0$ | $+\frac{3}{2} M \cos\theta - \frac{\sqrt{3}}{2} M \sin\theta + 1$ | -1 | $\frac{\sqrt{3}}{2} M \sin(\theta + \frac{\pi}{3}) - 1$ |
| $-2\pi/3 \leq \theta \leq -\pi/3$ | $\frac{\sqrt{3}}{2} M \cos(\theta + \frac{\pi}{6}) - 1$ | -1 | $-\frac{\sqrt{3}}{2} M \sin\theta - 1$ |
| $-\pi \leq \theta \leq -2\pi/3$ | -1 | $-\frac{\sqrt{3}}{2} M \cos(\theta + \frac{\pi}{6}) - 1$ | $-\frac{3}{2} M \cos\theta - \frac{\sqrt{3}}{2} M \sin\theta - 1$ |

Table 10: Average Leg voltages for **DPWM5**

| $60^0$ Sextant | Phase Leg a $\langle v_{az} \rangle / V_{dc}$ | Phase Leg b $\langle v_{bz} \rangle / V_{dc}$ | Phase Leg c $\langle v_{cz} \rangle / V_{dc}$ |
|---|---|---|---|
| $2\pi/3 < \theta < \pi$ | -1 | $-\frac{3}{2} M \cos\theta - \frac{\sqrt{3}}{2} M \sin\theta + 1$ | $-\frac{\sqrt{3}}{2} M \sin\theta - 1$ |
| $\pi/2 \leq \theta \leq 2\pi/3$ | $\frac{\sqrt{3}}{2} M \sin(\theta + \frac{\pi}{3}) - 1$ | $\frac{\sqrt{3}}{2} M \sin\theta - 1$ | -1 |
| $\pi/3 \leq \theta \leq \pi/2$ | $\frac{\sqrt{3}}{2} M \cos(\theta + \frac{\pi}{6}) + 1$ | 1 | $-\frac{\sqrt{3}}{2} M \sin\theta + 1$ |
| $0 \leq \theta \leq \pi/3$ | 1 | $-\frac{\sqrt{3}}{2} M \cos(\theta + \frac{\pi}{6}) + 1$ | $-\frac{3}{2} M \cos\theta - \frac{\sqrt{3}}{2} M \sin\theta + 1$ |
| $-\pi/3 \leq \theta \leq 0$ | $\frac{3}{2} M \cos\theta - \frac{\sqrt{3}}{2} M \sin\theta + 1$ | -1 | $\sqrt{3}\ M \sin(\theta + \frac{\pi}{3}) - 1$ |
| $-\pi/2 \leq \theta \leq -\pi/3$ | $\sqrt{3}\ M \cos(\theta + \frac{\pi}{6}) - 1$ | -1 | $-\sqrt{3}\ M \sin\theta - 1$ |
| $-2\pi/3 \leq \theta \leq -\pi/2$ | $\sqrt{3}\ M \sin(\theta + \frac{\pi}{3}) + 1$ | $\sqrt{3}\ M \sin\theta + 1$ | 1 |
| $-\pi \leq \theta \leq -2\pi/3$ | $\frac{3}{2} M \cos\theta + \frac{\sqrt{3}}{2} M \sin\theta + 1$ | $\sqrt{3}\ M \sin\theta + 1$ | 1 |

Table 11: Average Leg voltages for **DPWM6**

| $60^0$ Sextant | Phase Leg a $\langle v_{az} \rangle / V_{dc}$ | Phase Leg b $\langle v_{bz} \rangle / V_{dc}$ | Phase Leg c $\langle v_{cz} \rangle / V_{dc}$ |
|---|---|---|---|
| $3\pi/4 < \theta \le \pi$ | -1 | $-1-\sqrt{3}\ M\cos\left(\theta-\frac{\pi}{6}\right)$ | $-1+\sqrt{3}\ M\cos\left(\theta+\frac{5\pi}{6}\right)$ |
| $2\pi/3 < \theta \le 3\pi/4$ | $\frac{3}{2}M\cos\theta-\sqrt{3}M\sin\theta+1$ | 1 | $-\sqrt{3}M\sin\theta+1$ |
| $\pi/2 < \theta \le 2\pi/3$ | $\frac{\sqrt{3}}{2}\ M\cos(\theta+\frac{\pi}{6})+1$ | 1 | $\sqrt{3}M\sin\theta+1$ |
| $\pi/4 < \theta \le \pi/2$ | $-1-\sqrt{3}\ M\cos\left(\theta+\frac{5\pi}{6}\right)$ | $-1+\sqrt{3}\ M\sin\theta$ | -1 |
| $0 < \theta \le \pi/4$ | 1 | $-\frac{\sqrt{3}}{2}M\cos(\theta+\frac{\pi}{6})+1$ | $-\frac{3}{2}M\cos\theta-\sqrt{3}M\sin\theta+1$ |
| $-\pi/4 \le \theta \le 0$ | $-1+\sqrt{3}\ M\cos\left(\theta+\frac{\pi}{6}\right)$ | -1 | $-1-\sqrt{3}\ M\sin\theta$ |
| $-\pi/3 \le \theta < -\pi/4$ | 1 | $\sqrt{3}M\sin\theta+1-\frac{3}{2}M\cos\theta$ | $\frac{\sqrt{3}}{2}M\sin\theta+1$ |
| $-\pi/2 \le \theta < -\pi/3$ | $\frac{\sqrt{3}}{2}M\sin\left(\theta+\frac{\pi}{3}\right)+1$ | $\frac{\sqrt{3}}{2}\ M\sin\theta+1$ | 1 |
| $-3\pi/4 \le \theta < -\pi/2$ | $-1+\sqrt{3}\ M\cos\left(\theta+\frac{\pi}{6}\right)$ | -1 | $-1-\sqrt{3}\ M\sin\theta$ |
| $-\pi \le \theta < -3\pi/4$ | $\frac{3}{2}M\cos\theta+\frac{\sqrt{3}}{2}\ M\sin\theta+1$ | $\frac{\sqrt{3}}{2}\ M\sin\theta+1$ | 1 |

The overall harmonic losses for a particular modulation scheme can then be calculated by integrating the equation over a positive half fundamental cycle. For all modulation schemes, the phase leg reference voltages are the continuous function, and the integration can be done over one set of limits. For space vector modulation, the phase leg waveforms are separate sinusoidal segments in each $60^0$ sextants, for DPWMMIN as listed in Table 3.
Using the result given in [7],

$$\langle \Delta i_{ab}^{\ 2} \rangle = \left(\frac{Vdc}{L_\sigma}\right)^2 \frac{\Delta T^2}{48} \left\{(u_2-u_1)^2+(u_2-u_1)^3+(u_2-u_1)(u_2^{\ 3}-u_1^{\ 3})\right\} \qquad (23)$$

This is the generalized form of the ripple current equation,

Where $u_1=\frac{<v_{az}>}{Vdc}$, $u_2=\frac{<v_{bz}>}{Vdc}$ and $(u_1-u_2)=\frac{<v_{ab}>}{Vdc}$

and $L_\sigma = L_1+\frac{LmL_2}{Lm+L_2}$

the $L_1$, $L2$, and $Lm$ correspond to stator leakage, rotor leakage, and the magnetizing inductances respectively. The harmonic losses can then be determined by integrating equation over a positive half fundamental cycle (the above development is valid for $<v_{az}> > 0$), with appropriate

substitution for $u_1$ and $u_2$ for each modulation strategy to be evaluated, to determine the squared harmonic current ripple.

Substituting the values of $u_1$ & $u_2$ into equation (23) from the table for *DSVPWMs,* then creates separate expression for the squared harmonic ripple current over the positive fundamental cycle, gives the result that are[7]

## Existing Schemes

**$t_0 = 0$, $t_7 = 0$, DPWM0 and DPWM2**

$$I_{ab}{}^2{}_{,h,rms}{}_{M}{}^4 = \left(\frac{Vdc}{L_\sigma}\right)^2 \frac{\Delta T^2}{48}\left(6m^2 - \frac{35\sqrt{3}}{2\pi}m^3 + \left(\frac{27}{8} + \frac{81}{64}\frac{\sqrt{3}}{\pi}\right)m^4\right) \quad (24)$$

**DPWM 1**

$$I_{ab}{}^2{}_{,h,rms}{}_{M}{}^4 = \left(\frac{Vdc}{L_\sigma}\right)^2 \frac{\Delta T^2}{48}\left(6m^2 - \left(\frac{45}{2\pi} + \frac{4\sqrt{3}}{\pi}\right)m^3 + \left(\frac{27}{8} + \frac{27}{32}\frac{\sqrt{3}}{\pi}\right)m^4\right) \quad (25)$$

**DPWM 3**

$$I_{ab}{}^2{}_{,h,rms}{}_{M}{}^4 = \left(\frac{Vdc}{L_\sigma}\right)^2 \frac{\Delta T^2}{48}\left(6m^2 - \left(\frac{45}{2\pi} - \frac{31\sqrt{3}}{\pi}\right)m^3 + \left(\frac{27}{8} + \frac{27}{16}\frac{\sqrt{3}}{\pi}\right)m^4\right) \quad (26)$$

## Proposed Schemes

**DPWM 4**

$$I_{ab}{}^2{}_{,h,rms}{}_{M}{}^4 = \left(\frac{Vdc}{L_\sigma}\right)^2 \frac{\Delta T^2}{48}\left(\left(3\pi - \frac{9\sqrt{3}}{4}\right)m^2 + \left(\frac{-63\sqrt{3}}{32} - \frac{8.4563\sqrt{3}}{16}\right)m^3 + \left(\frac{81}{64\pi} - \frac{729\sqrt{3}}{512}\right)m^4\right) \quad (27)$$

**DPWM 5**

$$I_{ab}{}^2{}_{,h,rms}{}_{M}{}^4 = \left(\frac{Vdc}{L_\sigma}\right)^2 \frac{\Delta T^2}{48}\left(\left(\frac{297}{128\pi} + \frac{1647\sqrt{3}}{1024}\right)m^2 + \left(\frac{227\sqrt{3}}{116} - \frac{45}{4}\right)m^3 + \left(\frac{9}{2\pi} + \frac{9\sqrt{3}}{8}\right)m^4\right) \quad (28)$$

**DPWM 6**

$$I_{ab}{}^2{}_{,h,rms}{}_{M}{}^4 = \left(\frac{Vdc}{L_\sigma}\right)^2 \frac{\Delta T^2}{48}\left(\frac{4}{3\pi} + \left(-30\sqrt{3} + 12\sqrt{6} + 18\sqrt{2}\right)m + \left(\frac{27}{8} + \frac{111}{16\pi} - \frac{27\sqrt{3}}{4}\right)m^2 + \left(\frac{387\sqrt{2} + 357\sqrt{6}}{32} - \frac{2779\sqrt{3} + 1017}{64}\right)m^3 + \left(\frac{639\pi}{256} + \frac{243}{128} - \frac{1413\sqrt{3}}{1024}\right)m^4\right) \quad (29)$$

Or in more general terms as

$$I_{ab}{}^2{}_{,h,rms}{}_{M}{}^4 = \left(\frac{Vdc}{L_\sigma}\right)^2 \frac{\Delta T^2}{48}\, f(m) \quad (30)$$

Where the function *f(m)* is the *Harmonic distortion factor* **(HDF)**. HDF is commonly used as a figure of merit for PWM strategies that are independent of switching frequency, DC bus voltage, and load inductances. It only depends on the modulation index [6].The HDF for existing schemes are evaluated and are shown in Fig 9.

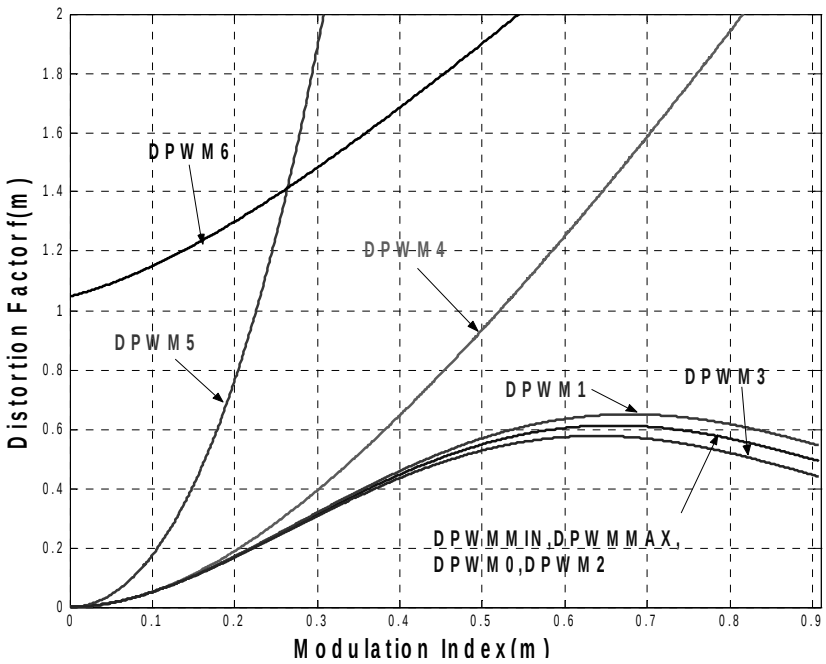


Fig. 9 Harmonic distortion factor *(HDF)* for different PWM strategies as a function of modulation index *(m)*, for pure inductive load

The superior performance of DPWM3 is seen from Fig. 9 for high modulation index among the existing scheme and DPWM1 can be considered worst for high modulation index. The zero vector i.e. $t_0$& $t_7$ can be kept zero only up to one sector, more than one sector may cause increase in switching losses as can be seen in DPWM5, in which the zero vector $t_0 = 0$ for first three sectors. The analysis of ripple current and plot with modulation index, results the ripples in output current increased.

Two more performance indices for comparison purpose are considered namely THD and WTHD in this paper. The method of comparing the effectiveness of modulation is by comparing the unwanted components i.e. the distortion in the output voltage or current waveform, relative to that of an ideal sine wave, it can be assumed that by proper control, the positive and negative portions of the output are symmetrical (no DC or even harmonics). The total harmonics distortion factor reduces to,

$$\text{THD} = \sqrt{\sum_{n=3,5,7..}^{\infty} \left(\frac{V_n}{V_1}\right)^2} \tag{31}$$

Normalizing this expression with respect to the quantity ($V_1$) i.e. fundamental, the weighted total harmonic distortion (WTHD) becomes defined as

$$\text{WTHD} = \frac{\sqrt{\sum_{n=3,5,7..}^{\infty} \left(\frac{V_n}{n}\right)^2}}{V_1} \tag{32}$$

The simulation is carried out to obtain THD and WTHD for different modulation index. The obtain results are given in Table 11a for the existing schemes and Table 11b for the proposed schemes. In simulation the switching period is taken as 0.2ms, and the inverter output frequency is designed as 50 Hz.

Table 12(a) - THD and WTHD of the existing schemes

| Mod. index | $t_0 = 0$ | | $t_7 = 0$ | | DPWM0 | | DPWM1 | | DPWM2 | | DPWM3 | |
|---|---|---|---|---|---|---|---|---|---|---|---|---|
| | THD | WTHD | THD | WTHD | THD | WTHD | THD | WTHD | THD | WTHD | THD | WTHD |
| 0.1 | 2.97 | 2.21 | 2.14 | 1.78 | 3.58 | 1.65 | 3.54 | 1.51 | 3.51 | 1.70 | 3.74 | 1.62 |
| 0.2 | 1.86 | 1.08 | 1.03 | 0.74 | 2.54 | 1.15 | 2.69 | 0.96 | 2.52 | 1.20 | 2.14 | 1.07 |
| 0.3 | 1.05 | 0.62 | 0.63 | 0.44 | 2.54 | 1.15 | 2.69 | 0.96 | 1.87 | 0.84 | 1.78 | 0.88 |
| 0.4 | 0.92 | 0.53 | 0.64 | 0.43 | 1.62 | 0.76 | 1.40 | 0.53 | 1.63 | 0.77 | 1.78 | 0.88 |
| 0.5 | 0.67 | 0.45 | 0.34 | 0.36 | 1.31 | 0.53 | 1.16 | 0.48 | 1.28 | 0.54 | 1.14 | 0.50 |
| 0.6 | 0.56 | 0.42 | 0.32 | 0.36 | 1.11 | 0.46 | 0.97 | 0.46 | 1.08 | 0.45 | 0.88 | 0.34 |
| 0.7 | 0.53 | 0.23 | 0.28 | 0.16 | 0.96 | 0.41 | 0.76 | 0.32 | 0.93 | 0.40 | 0.76 | 0.28 |
| 0.8 | 0.48 | 0.28 | 0.35 | 0.19 | 0.78 | 0.34 | 0.52 | 0.27 | 0.76 | 0.34 | 0.65 | 0.28 |
| 0.9 | 0.48 | 0.28 | 0.23 | 0.13 | 0.78 | 0.34 | 0.47 | 0.23 | 0.61 | 0.30 | 0.48 | 0.22 |
| 0.907 | 0.39 | 0.22 | 0.21 | 0.09 | 0.45 | 0.22 | 0.26 | 0.14 | 0.42 | 0.19 | 0.42 | 0.22 |

Table 12(b) - THD and WTHD of the proposed schemes

| Mod. index | DPWM4 | | DPWM5 | | DPWM6 | |
|---|---|---|---|---|---|---|
| | THD | WTHD | THD | WTHD | THD | WTHD |
| 0.1 | 3.21 | 2.01 | 3.81 | 2.26 | 4.02 | 2.12 |
| 0.2 | 2.47 | 1.21 | 2.41 | 1.21 | 2.59 | 1.09 |
| 0.3 | 1.56 | 0.81 | 1.87 | 0.94 | 2.51 | 0.84 |
| 0.4 | 1.57 | 0.76 | 1.42 | 0.79 | 1.67 | 0.80 |
| 0.5 | 1.11 | 0.54 | 1.31 | 0.58 | 1.50 | 0.61 |
| 0.6 | 0.91 | 0.47 | 1.11 | 0.44 | 1.23 | 0.55 |
| 0.7 | 0.84 | 0.35 | 0.90 | 0.33 | 0.98 | 0.37 |
| 0.8 | 0.76 | 0.34 | 0.68 | 0.42 | 0.74 | 0.42 |
| 0.9 | 0.57 | 0.27 | 0.68 | 0.42 | 0.60 | 0.27 |
| 0.907 | 0.37 | 0.21 | 0.46 | 0.25 | 0.45 | 0.20 |

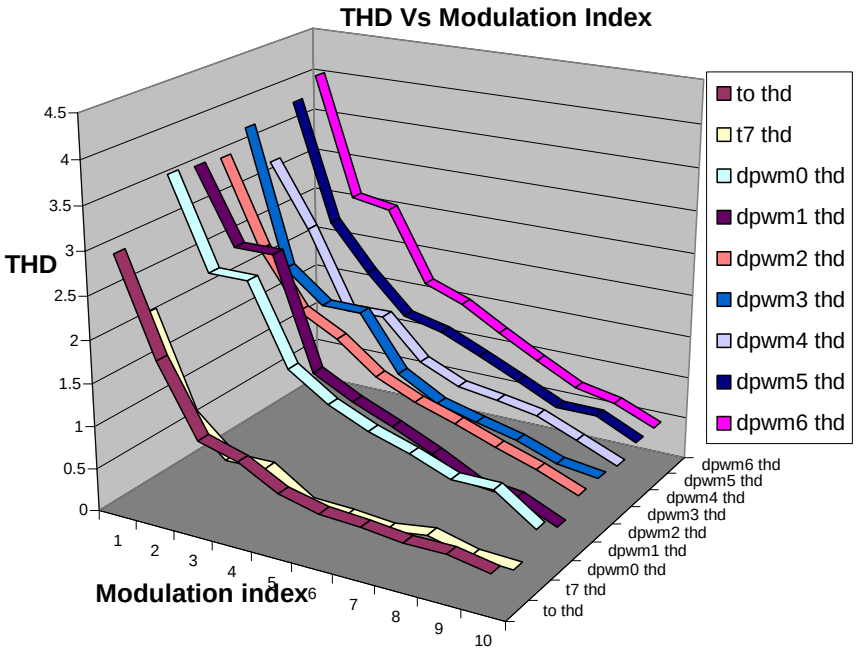


Fig.10 Total harmonic distortion (THD) for different modulation strategies as a function of modulation index (m) shows that THD decreases as the modulation index increases

The graphical representation of THD and WTHD is shown in Fig.10 for a quick comparison. Further, two more figures are generated at lowest and highest modulation index Fig11 and Fig 12.

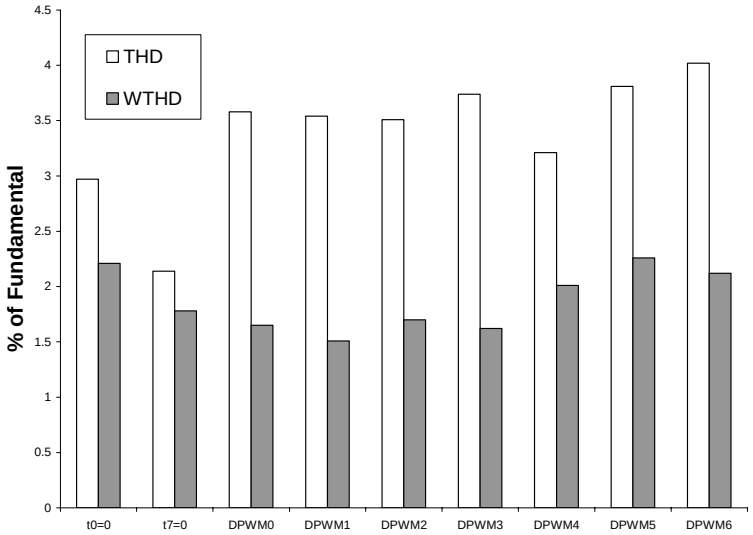


Fig 11 Comparison of THD & WTHD of different DSVPWM Schemes (at modulation index = 0.1)

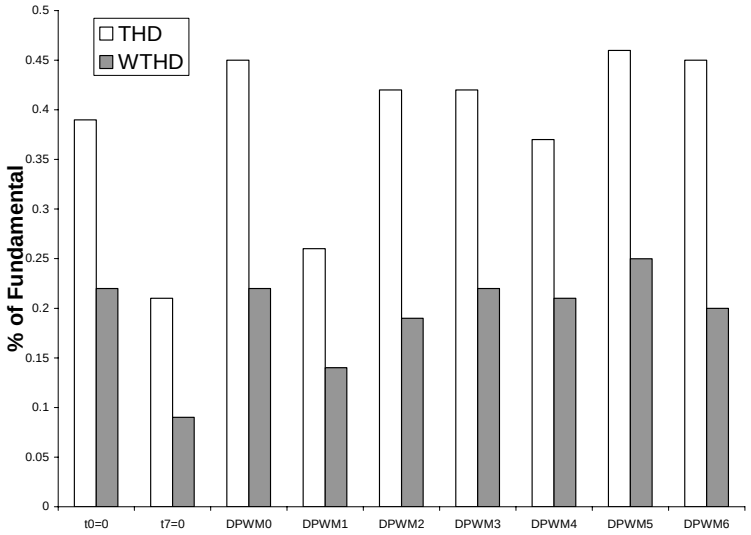


Fig 12 Comparison of THD & WTHD of different DSVPWM Schemes (at modulation index = 0.907)

At first the existing schemes are compared and it can be seen that THD and WTHD of the scheme $t_7$=0 is best than all other scheme, the schemes DPWM2 and DPWM3 give similar performance and the scheme DPWM0 is worst. In the proposed schemes DPWM4 is best and DPWM6 is worst.

To DSVPWM, using only one certain zero vector in the whole fundamental period will lead to the unbalance of switching frequency in the upper and lower arm, which would shorten the operation life of the inverter. However, two zero vectors are used in turns would not cause this problem. Furthermore, the THD decreases as the modulation increases, and the change is reversed when it comes to the continuous space vector PWM, this indicates that DSVPWM is more suitable to operate under the high modulation index.

Table 13(a) - THD and WTHD of the existing schemes at **unity** power factor

| Mod. index | $t_0 = 0$ | | $t_7 = 0$ | | DPWM0 | | DPWM1 | | DPWM2 | | DPWM3 | |
|---|---|---|---|---|---|---|---|---|---|---|---|---|
| | THD | WTHD | THD | WTHD | THD | WTHD | THD | WTHD | THD | WTHD | THD | WTHD |
| 0.1 | 2.97 | 2.21 | 2.14 | 1.78 | 3.58 | 1.65 | 3.54 | 1.51 | 3.51 | 1.70 | 3.74 | 1.62 |
| 0.2 | 1.86 | 1.08 | 1.03 | 0.74 | 2.54 | 1.15 | 2.69 | 0.96 | 2.52 | 1.20 | 2.14 | 1.07 |
| 0.3 | 1.05 | 0.62 | 0.63 | 0.44 | 2.54 | 1.15 | 2.69 | 0.96 | 1.87 | 0.84 | 1.78 | 0.88 |
| 0.4 | 0.92 | 0.53 | 0.64 | 0.43 | 1.62 | 0.76 | 1.40 | 0.53 | 1.63 | 0.77 | 1.78 | 0.88 |
| 0.5 | 0.67 | 0.45 | 0.34 | 0.36 | 1.31 | 0.53 | 1.16 | 0.48 | 1.28 | 0.54 | 1.14 | 0.50 |
| 0.6 | 0.56 | 0.42 | 0.32 | 0.36 | 1.11 | 0.46 | 0.97 | 0.46 | 1.08 | 0.45 | 0.88 | 0.34 |
| 0.7 | 0.53 | 0.23 | 0.28 | 0.16 | 0.96 | 0.41 | 0.76 | 0.32 | 0.93 | 0.40 | 0.76 | 0.28 |
| 0.8 | 0.48 | 0.28 | 0.35 | 0.19 | 0.78 | 0.34 | 0.52 | 0.27 | 0.76 | 0.34 | 0.65 | 0.28 |
| 0.9 | 0.48 | 0.28 | 0.23 | 0.13 | 0.78 | 0.34 | 0.47 | 0.23 | 0.61 | 0.30 | 0.48 | 0.22 |
| 1.0 | 0.39 | 0.22 | 0.21 | 0.09 | 0.45 | 0.22 | 0.26 | 0.14 | 0.42 | 0.19 | 0.42 | 0.22 |

Table 13(b) - THD and WTHD of the proposed schemes at **unity** power factor

| Mod. index | DPWM4 | | DPWM5 | | DPWM6 | |
|---|---|---|---|---|---|---|
| | THD | WTHD | THD | WTHD | THD | WTHD |
| 0.1 | 3.21 | 2.01 | 3.81 | 2.26 | 4.02 | 2.12 |
| 0.2 | 2.47 | 1.21 | 2.41 | 1.21 | 2.59 | 1.09 |
| 0.3 | 1.56 | 0.81 | 1.87 | 0.94 | 2.51 | 0.84 |
| 0.4 | 1.57 | 0.76 | 1.42 | 0.79 | 1.67 | 0.80 |
| 0.5 | 1.11 | 0.54 | 1.31 | 0.58 | 1.50 | 0.61 |
| 0.6 | 0.91 | 0.47 | 1.11 | 0.44 | 1.23 | 0.55 |
| 0.7 | 0.84 | 0.35 | 0.90 | 0.33 | 0.98 | 0.37 |
| 0.8 | 0.76 | 0.34 | 0.68 | 0.42 | 0.74 | 0.42 |
| 0.9 | 0.57 | 0.27 | 0.68 | 0.42 | 0.60 | 0.27 |
| 1.0 | 0.37 | 0.21 | 0.46 | 0.25 | 0.45 | 0.20 |

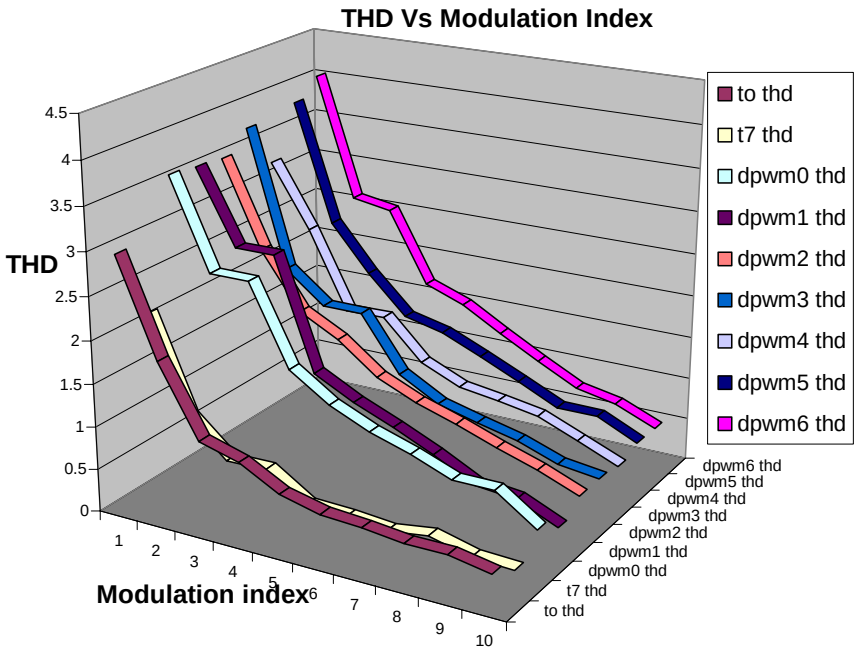


Fig.13 Total harmonic distortion (THD) for different modulation strategies as a function of modulation index (m) shows that THD decreases as the modulation index increases

Table 14(a) - THD and WTHD of the existing schemes at **30 deg. lagging** power factor

| Mod. index | $t_0 = 0$ | | $t_7 = 0$ | | DPWM0 | | DPWM1 | | DPWM2 | | DPWM3 | |
|---|---|---|---|---|---|---|---|---|---|---|---|---|
| | THD | WTHD | THD | WTHD | THD | WTHD | THD | WTHD | THD | WTHD | THD | WTHD |
| 0.1 | 0.94 | 1.03 | 0.95 | 1.02 | 0.71 | 0.51 | 0.67 | 0.46 | 0.75 | 0.55 | 0.75 | 0.48 |
| 0.2 | 0.41 | 0.42 | 0.42 | 0.42 | 0.46 | 0.34 | 0.40 | 0.26 | 0.47 | 0.38 | 0.46 | 0.36 |
| 0.3 | 0.26 | 0.23 | 0.27 | 0.23 | 0.31 | 0.24 | 0.26 | 0.19 | 0.32 | 0.26 | 0.35 | 0.26 |
| 0.4 | 0.22 | 0.19 | 0.23 | 0.19 | 0.29 | 0.23 | 0.22 | 0.15 | 0.30 | 0.24 | 0.35 | 0.27 |
| 0.5 | 0.17 | 0.20 | 0.19 | 0.22 | 0.21 | 0.16 | 0.19 | 0.15 | 0.20 | 0.16 | 0.20 | 0.15 |
| 0.6 | 0.16 | 0.19 | 0.18 | 0.22 | 0.18 | 0.14 | 0.20 | 0.17 | 0.17 | 0.14 | 0.14 | 0.10 |
| 0.7 | 0.10 | 0.07 | 0.10 | 0.08 | 0.16 | 0.12 | 0.13 | 0.09 | 0.16 | 0.12 | 0.12 | 0.07 |
| 0.8 | 0.11 | 0.10 | 0.12 | 0.09 | 0.13 | 0.10 | 0.13 | 0.09 | 0.13 | 0.10 | 0.13 | 0.08 |
| 0.9 | 0.11 | 0.11 | 0.09 | 0.07 | 0.12 | 0.10 | 0.11 | 0.08 | 0.11 | 0.09 | 0.11 | 0.07 |
| 1.0 | 0.06 | 0.06 | 0.09 | 0.08 | 0.09 | 0.09 | 0.06 | 0.06 | 0.10 | 0.08 | 0.08 | 0.06 |

Table 14(b) - THD and WTHD of the proposed schemes at **30 deg. lagging** power factor

| Mod. index | DPWM4 | | DPWM5 | | DPWM6 | |
|---|---|---|---|---|---|---|
| | THD | WTHD | THD | WTHD | THD | WTHD |
| 0.1 | 0.97 | 0.77 | 0.88 | 0.91 | 0.87 | 0.73 |
| 0.2 | 0.47 | 0.38 | 0.43 | 0.41 | 0.47 | 0.31 |
| 0.3 | 0.34 | 0.28 | 0.35 | 0.37 | 0.35 | 0.24 |
| 0.4 | 0.28 | 0.24 | 0.29 | 0.31 | 0.31 | 0.28 |
| 0.5 | 0.231 | 0.18 | 0.22 | 0.18 | 0.24 | 0.20 |
| 0.6 | 0.19 | 0.16 | 0.18 | 0.13 | 0.21 | 0.22 |
| 0.7 | 0.13 | 0.09 | 0.13 | 0.09 | 0.15 | 0.11 |
| 0.8 | 0.13 | 0.10 | 0.15 | 0.17 | 0.15 | 0.16 |
| 0.9 | 0.10 | 0.08 | 0.12 | 0.12 | 0.11 | 0.08 |
| 1.0 | 0.10 | 0.08 | 0.07 | 0.05 | 0.09 | 0.09 |

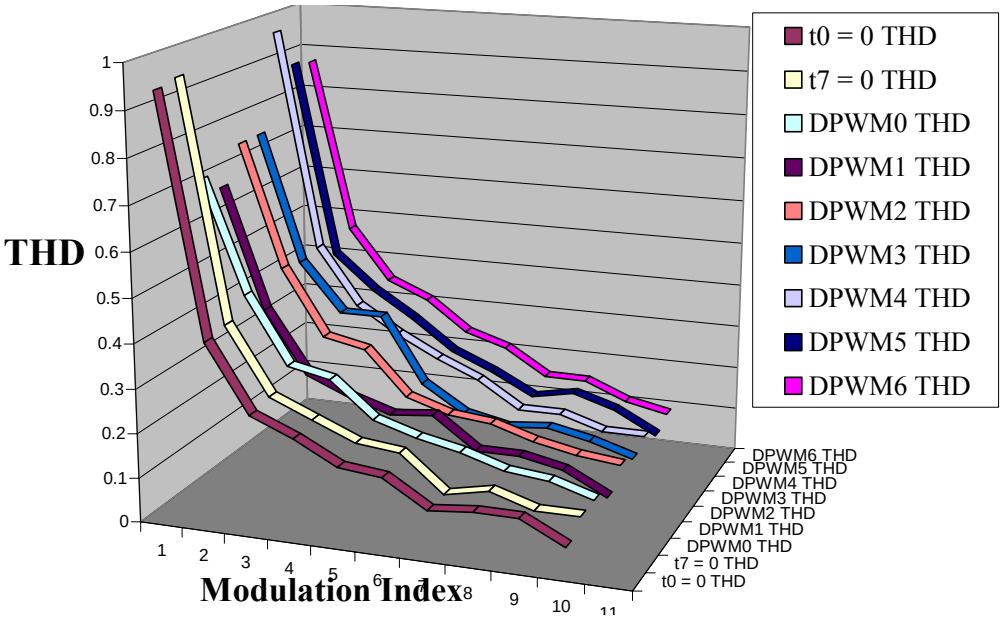


Fig.14 Total harmonic distortion (THD) for different modulation strategies as a function of modulation index (m) shows that THD decreases as the modulation index increases

Table 15(a) - THD and WTHD of the existing schemes at **60 deg. lagging** power factor

| Mod. index | $t_0 = 0$ | | $t_7 = 0$ | | DPWM0 | | DPWM1 | | DPWM2 | | DPWM3 | |
|---|---|---|---|---|---|---|---|---|---|---|---|---|
| | THD | WTHD | THD | WTHD | THD | WTHD | THD | WTHD | THD | WTHD | THD | WTHD |
| 0.1 | 0.62 | 0.70 | 0.63 | 0.71 | 0.43 | 0.33 | 0.40 | 0.30 | 0.45 | 0.35 | 0.45 | 0.30 |
| 0.2 | 0.26 | 0.28 | 0.27 | 0.28 | 0.28 | 0.22 | 0.24 | 0.17 | 0.29 | 0.24 | 0.28 | 0.23 |
| 0.3 | 0.17 | 0.15 | 0.17 | 0.15 | 0.19 | 0.16 | 0.16 | 0.13 | 0.19 | 0.17 | 0.21 | 0.17 |
| 0.4 | 0.14 | 0.12 | 0.14 | 0.13 | 0.18 | 0.15 | 0.13 | 0.10 | 0.18 | 0.16 | 0.22 | 0.17 |
| 0.5 | 0.11 | 0.13 | 0.13 | 0.15 | 0.12 | 0.10 | 0.11 | 0.10 | 0.12 | 0.10 | 0.12 | 0.10 |
| 0.6 | 0.11 | 0.13 | 0.13 | 0.15 | 0.11 | 0.10 | 0.13 | 0.11 | 0.11 | 0.09 | 0.08 | 0.06 |
| 0.7 | 0.06 | 0.05 | 0.07 | 0.05 | 0.10 | 0.08 | 0.08 | 0.07 | 0.09 | 0.08 | 0.07 | 0.04 |
| 0.8 | 0.07 | 0.07 | 0.07 | 0.05 | 0.08 | 0.07 | 0.08 | 0.07 | 0.08 | 0.06 | 0.08 | 0.05 |
| 0.9 | 0.07 | 0.08 | 0.05 | 0.04 | 0.07 | 0.07 | 0.07 | 0.05 | 0.07 | 0.06 | 0.07 | 0.05 |
| 0.907 | 0.04 | 0.04 | 0.05 | 0.05 | 0.07 | 0.07 | 0.04 | 0.04 | 0.06 | 0.05 | 0.05 | 0.04 |

Table 15(b) - THD and WTHD of the proposed schemes at **60 deg. lagging** power factor

| Mod. index | DPWM4 | | DPWM5 | | DPWM6 | |
|---|---|---|---|---|---|---|
| | THD | WTHD | THD | WTHD | THD | WTHD |
| 0.1 | 0.61 | 0.49 | 0.56 | 0.61 | 0.52 | 0.47 |
| 0.2 | 0.29 | 0.24 | 0.27 | 0.27 | 0.29 | 0.19 |
| 0.3 | 0.21 | 0.18 | 0.23 | 0.25 | 0.21 | 0.15 |
| 0.4 | 0.17 | 0.15 | 0.198 | 0.21 | 0.19 | 0.18 |
| 0.5 | 0.13 | 0.12 | 0.13 | 0.12 | 0.14 | 0.13 |
| 0.6 | 0.12 | 0.11 | 0.11 | 0.09 | 0.14 | 0.15 |
| 0.7 | 0.08 | 0.06 | 0.08 | 0.06 | 0.09 | 0.07 |
| 0.8 | 0.08 | 0.07 | 0.10 | 0.11 | 0.10 | 0.10 |
| 0.9 | 0.06 | 0.06 | 0.08 | 0.08 | 0.07 | 0.06 |
| 0.907 | 0.06 | 0.05 | 0.04 | 0.04 | 0.06 | 0.06 |

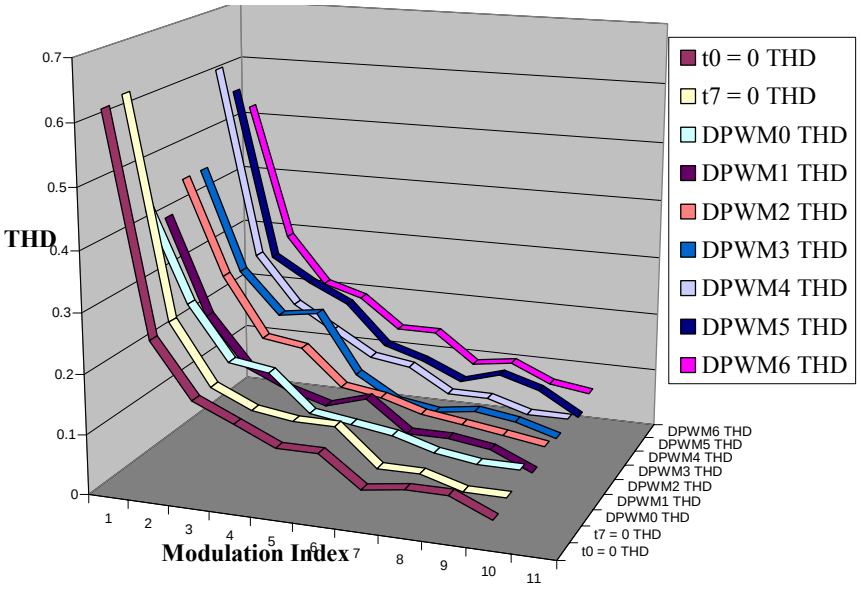


Fig.15 Total harmonic distortion (THD) for different modulation strategies as a function of modulation index (m) shows that THD decreases as the modulation index increases

Table 16(a) - THD and WTHD of the existing schemes at **90 deg. lagging** power factor

| Mod. index | $t_0 = 0$ | | $t_7 = 0$ | | **DPWM0** | | **DPWM1** | | **DPWM2** | | **DPWM3** | |
|---|---|---|---|---|---|---|---|---|---|---|---|---|
| | THD | WTHD | THD | WTHD | THD | WTHD | THD | WTHD | THD | WTHD | THD | WTHD |
| 0.1 | 0.53 | 0.52 | 0.57 | 0.52 | 0.37 | 0.28 | 0.35 | 0.26 | 0.40 | 0.31 | 0.39 | 0.26 |
| 0.2 | 0.27 | 0.21 | 0.23 | 0.14 | 0.24 | 0.19 | 0.21 | 0.14 | 0.25 | 0.21 | 0.25 | 0.20 |
| 0.3 | 0.26 | 0.27 | 0.22 | 0.20 | 0.17 | 0.13 | 0.14 | 0.11 | 0.17 | 0.15 | 0.19 | 0.15 |
| 0.4 | 0.23 | 0.25 | 0.19 | 0.19 | 0.15 | 0.13 | 0.11 | 0.08 | 0.16 | 0.14 | 0.19 | 0.15 |
| 0.5 | 0.10 | 0.12 | 0.11 | 0.13 | 0.11 | 0.09 | 0.10 | 0.08 | 0.11 | 0.09 | 0.11 | 0.09 |
| 0.6 | 0.12 | 0.14 | 0.15 | 0.17 | 0.09 | 0.08 | 0.11 | 0.10 | 0.09 | 0.08 | 0.07 | 0.05 |
| 0.7 | 0.07 | 0.08 | 0.08 | 0.08 | 0.08 | 0.07 | 0.07 | 0.05 | 0.08 | 0.07 | 0.06 | 0.04 |
| 0.8 | 0.11 | 0.13 | 0.13 | 0.14 | 0.07 | 0.06 | 0.07 | 0.06 | 0.07 | 0.05 | 0.07 | 0.04 |
| 0.9 | 0.14 | 0.17 | 0.11 | 0.13 | 0.06 | 0.06 | 0.06 | 0.04 | 0.06 | 0.05 | 0.06 | 0.04 |
| 0.907 | 0.04 | 0.04 | 0.06 | 0.07 | 0.05 | 0.05 | 0.03 | 0.04 | 0.05 | 0.04 | 0.04 | 0.03 |

Table 16(b) - THD and WTHD of the proposed schemes at **90 deg. lagging** power factor

| Mod. index | **DPWM4** | | **DPWM5** | | **DPWM6** | |
|---|---|---|---|---|---|---|
| | THD | WTHD | THD | WTHD | THD | WTHD |
| 0.1 | 0.54 | 0.43 | 0.50 | 0.54 | 0.45 | 0.42 |
| 0.2 | 0.25 | 0.21 | 0.23 | 0.24 | 0.25 | 0.17 |
| 0.3 | 0.18 | 0.16 | 0.20 | 0.22 | 0.19 | 0.13 |
| 0.4 | 0.15 | 0.13 | 0.16 | 0.19 | 0.17 | 0.16 |
| 0.5 | 0.11 | 0.10 | 0.12 | 0.10 | 0.13 | 0.12 |
| 0.6 | 0.11 | 0.09 | 0.10 | 0.07 | 0.12 | 0.13 |
| 0.7 | 0.07 | 0.05 | 0.07 | 0.05 | 0.08 | 0.06 |
| 0.8 | 0.07 | 0.06 | 0.09 | 0.10 | 0.09 | 0.19 |
| 0.9 | 0.05 | 0.05 | 0.07 | 0.07 | 0.06 | 0.04 |
| 0.907 | 0.05 | 0.05 | 0.04 | 0.03 | 0.05 | 0.06 |

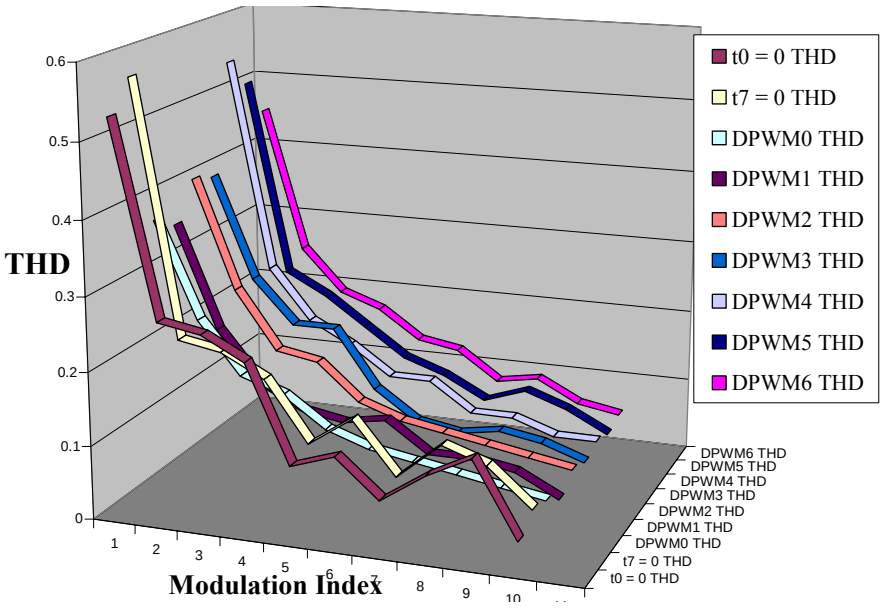


Fig.16 Total harmonic distortion (THD) for different modulation strategies as a function of modulation index (m) shows that THD decreases as the modulation index increases

## (6)Conclusions

By arranging the two zero vectors skillfully space vector method named DSVPWM for three phase inverter is analyzed in this paper. Under the same situation, allows the switching frequency to increase by a nominal value of 3/2 accordingly for the same inverter losses. The switching losses of DSVPWM are one fifth less than continuous space vector, and if the parameter of load matches the PWM pattern, the switching loss will reduce further. There are six different DPWM are available in the literature .A comprehensive analysis of these existing DPWM is done and reported in the paper. Analytical and simulation results are incorporated. Three novel schemes are suggested by skillfully placing the zero vectors. Simulation studies are done to evaluate the performance of the proposed methods.

Any sector can be divided in equal parts e.g. DPWM2 & DPWM3 will not cause increase in switching losses, but if the distribution is unequal as in the case of DPWM4 & DPWM6 will cause increase in losses. By analysis of all the schemes we find that, the sector must be divided in equal parts may be 2,4,6,…, but not in unequal parts, which increase the switching losses. The maximum range of keeping the zero vectors zero is only one sector and if we keep it zero more than one sector in continuation, the losses will suddenly increase.

For pure inductive load the best existing scheme is seen as DPWMMIN and worst is DPWM1. Among the proposed schemes DPWM4 is providing lower THD and WTHD. However the proposed scheme DPWM4 is better than existing schemes DPWMMAX, DPWM0, DPWM2 and DPWM3. The performance of modulators for different loading conditions can be done.

## (7) References


[1]. J. Holtz, "Pulse width modulation- a survey", *IEEE Trans. On Industrial Electronics*, vol. 39, issue 5, pp. 410-420, Oct. 1992.

[2]. J.Holtz, "Pulse width modulation for electronic power conversion", *Proc. IEEE* vol. 8., pp. 1194-1214, Aug. 1994.

[3]. J.A. Houdsworth and D.A. Grant, "The use of harmonic distortion to increase output voltage of a three-phase PWM inverter", *IEEE Trans. Industry Appl.,* vol. IA-20, pp. 1124-1228, sept./oct. 1984.

[4]. M. Depenbrock, "Pulse width control of a three-phase inverter with non sinusoidal phase voltage of a three-phase PWM inverter", *Proc. IEEE Int. semiconductor Power Conversion Conf.* , pp. 399-403, 1977.

[5]. J.W. Kolar, H. Ertl and F.C. Zach, "Influence of the modulation methods on the conduction and switching losses of a PWM converter system", *IEEE Trans. Industry Appl.* vol. 27, pp. 1063-1975, Nov./Dec. 1991.

[6]. A.M.Hava, R.J.Kerkman and T.A. Lipo, "A High performance Generalized discontinuous PWM algorithm", *IEEE Trans. On Industry Appl.,* vol. 34, no. 5, sept./oct., 1998.

[7]. D. Grahame Holmes and T. A. Lipo , "*Pulse Width Modulation For Power Converters – Principles and Practices*", *IEE Press*, Wiley Publications, 2000.

[8]. M.P. Kazmierkowski, R. Krishnan and F. Blaabjerg, "*Control in power electronics-selected problems", Academic Press*, California, USA, 2002.

[9]. G. Dong, "Sensorless and efficiency optimized induction motor control with associated converter PWM schemes", *PhD Thesis,* Faculty of Graduate School, Tennessee Technological University, Dec. 2005.

[10]. A.M. Hava, "Carrier based PWM-VSI drives in the overmodulation region", *PhD Thesis*, University of Wisconsin-Medison, 1998.
[11]. H.W. van de Broeck, H.C. Skudelny and G.V. Stanke, "Analysis and realization of a pulsewidth modulator based on space vectors", *IEEE Tarns. Industry Appl.,* vol. 24, pp. 142-150, Feb. 1988.
[12]. D.G. Holmes, "The significance of zero space vector placement for carrier-based PWM schemes", *IEEE Trans. Industry Appl.,* vol. 32, no. 5, pp. 1122-1129 sept./oct 1996.
[13]. K. Zhou and D. Wang, "Relationship between space vector modulation and three phase carrier based PWM – A comprehensive analysis", *IEEE Trans. on Ind. Elect.*, vol. 49, no. 1, Feb-2002.
[14]. Bimal K Bose, "Modern Power Electronics and Drives," PHI publication-2002.
[15]. K. Taniguchi , Y. Ogino and H. Irie, " PWM techniques for power MOSFET inverter," *IEEE Trans. Power Electronics*, vol. 3, pp. 328-334, July 1998.